PICOSCALE Vibrometer System Controller PV-CTRL-V1.5

The system controller hosts all the necessary optical components and electronics to generate the IR laser beam and to detect the interference signal. Furthermore, it contains the circuitry to convert the measured interferometric data into a position signal and to extract its amplitude and frequency.
This document contains the general specifications of the system controller. Refer to the dedicated specification sheet for a detailed description of the performance limitations of the system controller.

Table 1. *Interferometer specifications.*

Property	Value
Channels	1
Measurement laser	(1545±15) nm, laser class 1
Measurement laser accuracy	$< 10^{-6}\mathrm{m/m}$
Pilot laser	(650±5) nm, laser class 1
Periodic nonlinearities*	$< 8\mathrm{nm}_{\mathrm{peak-to-peak}}$
Resolution and noise	cf. Table
Max. target velocity	1 m/sec
Max. bandwidth	2.9 MHz
Max. data rate	10 MHz
Target Reflectivity	4%-100%, $\lambda_{1550\mathrm{nm}}$
Target object features size**	$\geqslant r_{lateral}$
Measurement conditions***	ambient, ultra-high vacuum

* Valid for PV-SH-F03 with NA0.15, NA0.25 and NA0.05 objectives
** $r_{lateral}$ depends on the objective used. Refer to the corresponding specification sheet.
*** Depending on the PV-XYZ and PV-SH properties.

GENERAL PERFORMANCE

The key specifications of the system controller are summarized in Table 1 and references therein. All data are typical values and have been inferred from careful characterization measurements. They strongly depend on the setup the **PICO**SCALE *Vibrometer* is used in. Please contact SmarAct to discuss your application and possible limitations. We will be happy to assist you on your way to get the maximum out of your device and will also be able to provide detailed feasibility studies.

Resolution

The resolution of a position measurement is the position change that can be clearly identified. It depends on different influences; digital influences like the resolution of the analog-to-digital converters, but also and mainly on the performance of the analog system. There are minute fluctuations caused by noise inside the sensor signal even if the observed object is at rest. The noise can be described by spectral densities. We use in the following the so called amplitude spectral density $\mathrm{ASD(f)}$. The ASD can be converted to RMS noise values by integration over the desired frequency range:

$$\delta(f_{min}, f_{max}) = \sqrt{\int_{f_{min}}^{f_{max}} [\mathrm{ASD(f)}]^2 \, \mathrm{df}} \qquad (1)$$

Digital Resolution

The digital system of the system controller uses 16bit ADC signals. These ADC values are further processed and 48bit position values are generated. Due to internal oversampling and corresponding averaging, the digital resolution of the PicoScale is 1 pm even at 10 MHz streaming frequency.

Noise characterization - working distance

The position noise of a measurement with the **PICO**SCALE *Vibrometer* is determined by several contributions, which can partially be attributed to the system controller and its electronics, as well as noise and/or distortions induced by the measurement setup (thermal drift, mechanical vibration, air fluctuations, etc.). In the quantification of a high resolution measurement device like the **PICO**SCALE *Vibrometer*, care must be taken to exclude the presence of the latter in order not to underestimate the capabilities of the measurement device itself.
The system controller contains a distributed feedback (DFB) laser which has a certain linewidth. The phase noise of the laser contributes to the position noise. The position noise increases with working distance, since the phase noise adds up for longer ranges.
In Figure 1 the amplitude spectral densities of a few measurements at different working distances are dis-

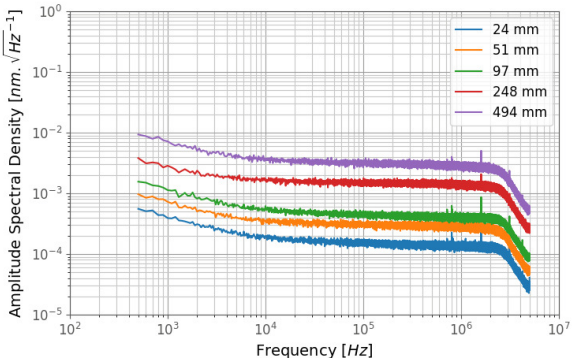

Figure 1. *Typical amplitude spectral density of a position measurement with high working distances (WD). Acoustic and mechanical noise adds to the curve at frequencies below 1 kHz and must not be attributed to the measurement device itself. (Sample frequency 10 MHz, FFT block size 50000, 100 averages, Rectangular window.)*

played.
If the working distance increases, so does the noise floor due to laser phase noise. This effect has been measured with different working distances between 15 mm to 0.5 m. The results are summarized in Figure 2. As expected, the noise increases linearly with the distance.

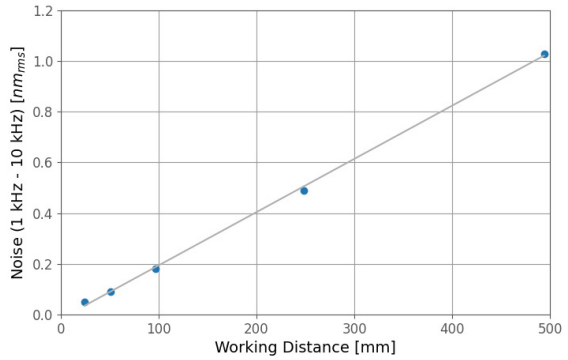

Figure 2. *Root-mean-square (rms) noise in the frequency band (1 kHz, 10 kHz) for different working distances. The noise increases linearly with working distance due to laser phase noise.*

Noise characterization - frequency dependency
In Figure 3, the amplitude spectral density of a position measurement with a monolithic interferometer is shown. The graph shows three spectra, recorded with sample rates of 1.2 kHz, 312.5 kHz and 10 MHz. The gray line represents an empirical model that can be used to estimate the noise for frequencies >1 Hz. It is given by the formula:

$$ASD_m(f, WD_R)\left[\frac{pm}{\sqrt{Hz}}\right] = WD_R\left(0.2 + \sqrt{\frac{375^2}{15^2 + f^2}}\right) \quad (2)$$

where f is the sideband frequency and $WD_R = \frac{1.5 * X}{20 mm}$ with X is actual the working distance.

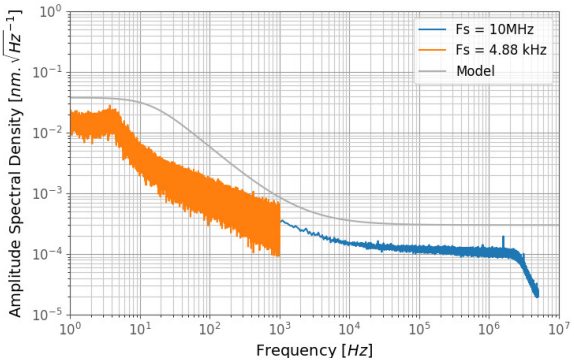

Figure 3. *Amplitude spectral density of a position measurement with a monolithic setup at a working distance of 50 mm but normalised to 20 mm. (Sample frequency 4.88 kHz and 10 MHz with 10 and 100 averages respectively. Both uses rectangular windowing.)*

The data of Figure 3 can be used to estimate the RMS noise in different frequency bands. The total noise over all bands is given by[1]

$$\Delta = \sqrt{\sum_{f_{min}, f_{max}} \delta(f_{min}, f_{max})^2}\,. \quad (3)$$

In Table 2 the RMS noise for a compact 35 mm long setup is summarized, which has a similar working distance than the PS-SH-F03 sensorheads.

Table 2. *Measured RMS values of the position noise in nm of the system controller per frequency decade and for a working distances of 35 mm, typical working distance for PV-SH-F03 sensorheads (black). The values in orange are calculated using Equation 2, and represent an **upper bound**. Please note that the model is only validated for frequencies above 1 Hz.*

Frequency Band	RMS noise, Typical	RMS noise, Model
0.01 Hz – 0.1 Hz	0.02 nm	-
0.1 Hz – 1 Hz	0.04 nm	-
1 Hz – 10 Hz	0.05 nm	0.19 nm
10 Hz – 100 Hz	0.04 nm	0.21 nm
100 Hz – 1 kHz	0.04 nm	0.11 nm
1 kHz – 10 kHz	0.04 nm	0.09 nm
10 kHz – 100 kHz	0.05 nm	0.16 nm
100 kHz – 1 MHz	0.16 nm	0.51 nm
1 MHz – 5 MHz	0.26 nm	1.05 nm
0.01 Hz – 5 MHz	**0.32 nm**	**1.23 nm**

[1] The noise contributions in each band are uncorrelated so that "the variance of the sum is the sum of variances".

Low pass filters

The system controller features low pass filters that limit the bandwidth and sufficiently reduce the noise in the system. The system filters can be set in 23 steps according to

$$f_{LP} \approx 2.3\,\text{MHz}/2^{n} \quad , n \in [1, 23] \tag{4}$$

(If no filter is set, n=0, the bandwidth is limited by a $f_{LP} = 2.9$ MHz analog low-pass filters.) For example, if one is able to limit the bandwidth to 10 kHz (n=8, $f_{LP} \approx$ 9 kHz), and the lowest frequency of interest is 1 Hz, one only need to add (acc. to Equation 3) the noise contributions of the four frequency bands (1 Hz, 10 Hz), (10 Hz, 100 Hz), (100 Hz, 1 kHz) and (1 kHz, 10 kHz). For a working distance of 0.1 m this gives a RMS noise of Δ =0.30 nm_{rms}, compared to Δ =1.17 nm_{rms} in the full band (0.01 Hz, 5 MHz).

Thermal stability

Within the system controller controller there are electronic components, which are generally sensitive to thermal stress, which may affect the laser wavelength stabilization and thus the accuracy. In order to quantify the effect of thermal stress on the actual position reading, the controller was placed in a climate chamber, and the temperature was cycled between 20 °C and 25 °C, see Figure 4.

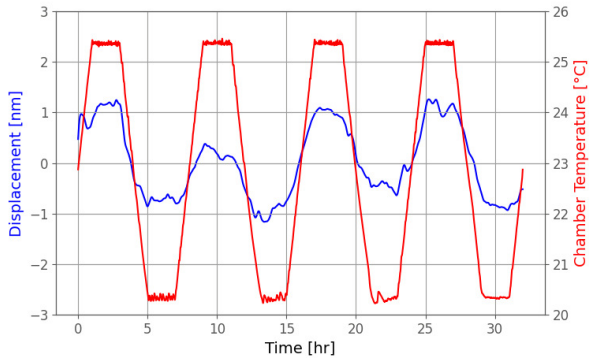

Figure 4. *Displacement data (blue) of a static setup when the system controller Controller is in a climate chamber, which is cycled ten times from 20.5 °C to 25.5 °C (gray).*

The sensor head and target were not in the chamber and did not experience the thermal stress. Consequently, all observed drift that correlates with the chamber temperature can be attributed to the controller[2]. We find, that the observed drift was below ±1 nm. The temperature dependence of the position reading is thus:

$$\frac{dx}{dT} = \frac{2\,\text{nm}}{5\,°\text{C}} = 0.4\,\text{nm}\,°\text{C}^{-1}\,. \tag{5}$$

Assuming that the temperature solely affects the laser wavelength[3], one can calculate the relative error by using the working distance of the setup (20 mm) as

$$\frac{d}{dT} = \frac{2\,\text{nm}}{20\,\text{mm}\cdot 5\,°\text{C}} = 0.02\,\text{ppm}\,°\text{C}^{-1}\,, \tag{6}$$

which is, for example, well below the thermal expansion coefficient of common materials in a setup (aluminum: 23 ppm/°C, iron: 12 ppm/°C, glass: 10 ppm/°C). Furthermore, the time constant of the effect is very long and other noise sources are typically orders of magnitudes stronger than the thermal effect on the controller electronics.

PERFORMANCE - VIBROMETRY SPECIFIC

In this section, the performance of the system with respect to the main operation modes of the **PICO**SCALE *Vibrometer* is discussed, namely:

- Microscopy: In this mode, the laser beam is raster-scanned over the target to retrieve reflection information and reconstruct a microscopy image.
- Topography: In this mode, the laser beam is raster-scanned over the target to retrieve topography information.
- *Local Analysis*: In this mode, the laser beam is steady and the local vibration, i-e on a point, is retrieved. The displacement signal is recorded and post-processed via Fourier transformation to dissect the local vibrational behavior.
- *Modal Analysis*: In this mode, the laser beam is raster-scanned over the target while the target is getting actuated. The displacement signal is demodulated to extract both the phase and amplitude of vibration with respect to the excitation signal. Vibrational mode can then be directly imaged.

Microscopy

Calibration factor

Periodic non-linearity

Microscopy information is retrieved from the relative reflectivity. Prior calculation of the relative reflectivity, internal routines ensure that the quadrature signals are normalized and properly in quadrature. The output relative reflectivity signal suffers however from periodic non-linear errors originating from erroneous corrections and presence of multipath interferences. These errors depend on the devices, the measurement objects and the environmental conditions.
In case of microscopy measurement, the periodic non-linear errors result in a periodic pattern within the microscopy image of period $\lambda_{1550\text{nm}}/2$ and $\lambda_{1550\text{nm}}/4$. The relative reflectivity fluctuates up to 5%.

[2] For details on this measurement please contact SmarAct.

[3] The impact on the laser wavelength is considered the worst case scenario, as other effects will not scale linearly with working distance.

Topography
To unambiguously estimate the measurement object height, the height between two neighboring pixels of the topography image should be below $\lambda_{1550nm}/2$, or ≈775 nm.

Resolution and accuracy
The resolution of the topography measurement is 50 nm and the accuracy is 250 nm.

Out-of-plane Vibration
Table 3 summarizes the different data sources available when measuring out-of-plane vibrations during *Local Analysis*.

Table 3. *Available data sources*

Data sources	f_s
Displacement	$\leqslant 10MHz$
Velocity	$\leqslant 10MHz$
Acceleration	$\leqslant 10MHz$
Analog In	$\leqslant 10MHz$

All data sources can be displayed and saved in either the time domain (raw data, unprocessed) or in the frequency domain (post-processed data).

Working frequency range
The working frequency range is summarized in Table 4.

Table 4. *Working frequency range*

Measurement	Δf
Local Analysis	$[DC : 2.5MHz]$
Modal Analysis	$[50Hz : 2.5MHz]$

In *Local Analysis*, the working frequency range is limited by the analogue lock-in amplifiers that extracts both quadrature signals. The cutoff frequency of the low-pass filters is 2.9 MHz at $-1dB$.
In *Modal Analysis*, the working frequency range is further reduced because of the dual-phase lock-in amplifier. Prior demodulation, the relative displacement signal is high-pass filtered. This high-pass filter has a corner frequency at $-3dB$ of 50 Hz.

Maximum measurement amplitude
In *Modal Analysis*, the maximum measurement amplitude is given by:

$$A_{max}[m] = \frac{\lambda_{1550nm}}{4} \cdot \frac{f_s}{2\pi \cdot f} \tag{7}$$

In *Local Analysis*, it is further limited by data compression:

$$A_{max}[m] = 2^{16} \cdot sdr \cdot \frac{f_s}{2\pi \cdot f} \tag{8}$$

Both maximum measurement amplitudes are shown in Table 5.

Table 5. *Maximum measurement amplitude at 10 MHz.*

f	Local A_{max}	Modal A_{max}
1Hz	104mm	617mm
10Hz	10mm	62mm
100Hz	1mm	6mm
1kHz	104µm	617µm
10kHz	10µm	62µm
100kHz	1µm	6µm
1MHz	104nm	617nm

The **PICO**SCALE *Vibrometer* uses confocal optics which further reduces the maximum measurement amplitude to the objective axial resolution.

Dual-phase lock-in amplifier bandwidth and time response
In *Modal Analysis*, the relative displacement signal serves as input for the dual-phase lock-in amplifier.
Table 6 summarizes the dual-phase lock-in amplifier performances at 10 MHz.

Table 6. *Specifications at $F_s = 10 MHz$*

Configuration	Δf_{10MHz}	τ_{10MHz}
Fine	16kHz	43.2µs
Narrow	32kHz	21.6µs
Normal	64kHz	10.8µs
Wide	128kHz	5.4µs

Both bandwidth and time response are affected by the downsampling rate of the decimator prior demodulation according to:

$$\begin{aligned} \Delta f_{fs} &= \Delta f_{10MHz} \cdot R^{-1}, \\ \tau_{fs} &= \tau_{10MHz} \cdot R \end{aligned} \tag{9}$$

Calibration factors
Wavelength uncertainty
The relative displacement, thus the amplitude of vibration, measured by a michelson-based vibrometer is directly proportional to the wavelength of the laser. The **PICO**SCALE *Vibrometer* uses a laser source which is stabilized to an absorption cell which is traceable to NIST standards. The error on the wavelength is given by $\lambda \cdot 10^{-6}$. The effect on the measurement is then

negligible within the measurement range.

Periodic non-linearity
The relative displacement signal suffers from periodic non-linear errors originating from erroneous corrections and presence of multipath interferences. These errors depend on the devices, the measurement objects and the environmental conditions. It is then only possible to provide a worst-case scenario which is taken as the limitation of the **PICO**SCALE *Vibrometer*. The worst-case scenario is a 8 nm-induced periodic non-linear error on the relative displacement signal that can sometimes occur if the system is not properly adjusted at focus. In most cases, it is much less than 5 nm. Under these conditions, the induced error on the amplitude of vibration is shown in Table 7.

Table 7. *Amplitude error from periodic non-linearity.*

Range	$\epsilon_{amplitude}$
1 pm - 10 pm	6%
10 pm - 100 pm	6%
100 pm - 1 nm	6%
1 nm - 10 nm	6%
10 nm - 100 nm	6%
100 nm - 1 µm	1%
1 µm - 10 µm	0.1%
10 µm - 100 µm	0.02%

Compensator
In *Modal Analysis*, the amplitude of vibration is extracted using a digital dual-phase lock-in amplifier. This digital component has been calibrated to compensated for induced damping. The amplitude error is less than 0.025% within the working frequency range.

Digital signal output jitter
In *Local Analysis*, it is possible to average multiple time series in a row. It exists however an intrinsic measurement jitter of less than 40 ns that will affect the measurement of the phase and amplitude of the vibrations:

$$\begin{aligned} \epsilon_{phase}[\%] &= \Delta_J \cdot f \cdot 100, \\ \epsilon_{amplitude}[\%] &= (1 - \cos(\Delta_J \cdot \pi \cdot f)) \cdot 100 \end{aligned} \quad (10)$$

Both errors are shows in Table 8.
In the frequency domain, the amplitude of vibration remains unaffected because of the incoherent averaging.

High-aperture effects
The **PICO**SCALE *Vibrometer* uses confocal optics which is sensitive to the Gouy phase shift. The impact of such phase shift depends on the sensor head in used but overall, the error on the amplitude of vibration will be less than 3.5% up to 100 µm vibration amplitude, see Table 9.

Table 8. *Error from the digital signal output jitter.*

f	ϵ_{phase}	$\epsilon_{amplitude}$
1 Hz	790f%	4µ%
10 Hz	79p%	40µ%
100 Hz	7.9n%	400µ%
1 kHz	790n%	4m%
10 kHz	79µ%	40m%
100 kHz	7.9m%	400m%
1 MHz	789m%	4%
5 MHz	19%	20%

Table 9. *Amplitude error from high-aperture effects.*

Sensor Head	$\epsilon_{amplitude,max}$
F03 NA0.15	0.25%
F03 NA0.25	0.80%
F03 NA0.50	3.50%

Influence of the medium
The **PICO**SCALE *Vibrometer* assumes that the interferometric laser beam travels through a medium of refractive index equals to 1. If the measurement object is fully contained within a medium of different index, the amplitude of vibration will be affected such that:

$$A_{true}[m] = A_{measured} \cdot n_i^{-1} \quad (11)$$

In air, the refractive index is 1.00027. The error is then negligible.

Influence of the measurement object tilt
The existence of tilt between measurement object and optical path affects the measurement of the true amplitude such that:

$$A_{true}[m] = A_{measured} \cdot \cos(\Theta) \quad (12)$$

The worst-case scenario occurs if the tilt equals the angular range of the sensor heads, see Table 10.

In-plane Vibration
Table 11 summarizes the different data sources available when measuring in-plane vibrations during *Local Analysis*.
All data sources can be displayed and saved in either the time domain (raw data, unprocessed) or in the frequency domain (post-processed data).

Table 10. *Amplitude error from measurement object tilt.*

Sensor Head	$\epsilon_{amplitude,max}$
F03 NA0.15	0.30%
F03 NA0.25	0.60%
F03 NA0.50	3.00%

Table 11. *Available data sources*

Data sources	f_s
Relative reflection	$\leqslant$ 5MHz
Analog In	$\leqslant$ 10MHz

Working frequency range

In *Stroboscopic Analysis*, the working frequency range is limited by the analogue lock-in amplifiers that extracts both quadrature signals. The cutoff frequency of the low-pass filters is 2.5 MHz at −1 dB.

In *Knife-edge Analysis*, the working frequency range is futher reduced because of the dual-phase lock-in amplifier. Prior demodulation, the relative reflection signal is high-pass filtered. This high-pass filter has a corner frequency at −3 dB of 50 Hz.

The working frequency range for each analysis is displayed in Table 12.

Table 12. *Working frequency range*

Measurement	Δf
Stroboscopic Analysis	[DC : 2.5MHz]
Knife-edge Analysis	[50 : 2.5MHz]

Maximum measurement amplitude

In *Modal Analysis*, the maximum measurement amplitude is given by:

$$A_{max}[m] = \frac{\lambda_{1550nm}}{4} \cdot \frac{f_s}{2\pi \cdot f} \tag{13}$$

In *Local Analysis*, it is further limited by data compression:

$$A_{max}[m] = 2^{16} \cdot sdr \cdot \frac{f_s}{2\pi \cdot f} \tag{14}$$

Both maximum measurement amplitudes are shown in Table 13.

Dual-phase lock-in amplifier bandwidth and time response

In *Knife-edge Analysis*, the relative reflection signal serves as input signal for the dual-phase lock-in amplifier.

Table 14 summarizes the dual-phase lock-in amplifier performances at 10 MHz.

Both bandwidth and time response are affected by the downsampling rate of the decimator prior demodulation according to:

$$\begin{aligned} \Delta f_{fs} &= \Delta f_{10MHz} \cdot R^{-1}, \\ \tau_{fs} &= \tau_{10MHz} \cdot R \end{aligned} \tag{15}$$

Table 13. *Maximum measurement amplitude at 5 MHz.*

f	Local A_{max}	Modal A_{max}
1 Hz	51mm	308mm
10 Hz	5mm	31mm
100 Hz	512µm	3mm
1 kHz	51µm	308µm
10 kHz	5µm	31µm
100 kHz	512nm	3µm
1 MHz	51nm	308nm

Table 14. *Specifications at F_s = 10 MHz*

Configuration	Δf_{10MHz}	τ_{10MHz}
Fine	16kHz	43.2 µs
Narrow	32kHz	21.6 µs
Normal	64kHz	10.8 µs
Wide	128kHz	5.4 µs

Calibration factors

Positioning system

The in-plane vibration amplitude is directly proportional to the pixel size. It is then dependent on the positioning system accuracy. The error on the lateral amplitude for a CLS-3232 is less than 1%.

However, the calculation of the lateral amplitude depends also on the post-processing of the sequential images. The stated accuracy for the template matching algorithm used is 15%.

Digital signal output jitter

In *Local Analysis*, it is possible to average multiple time series in a row. It exists however an intrinsic measurement jitter of less than 40 ns that will affect the measurement of the phase and amplitude of the vibrations:

$$\begin{aligned} \epsilon_{phase}[\%] &= \Delta_J \cdot f \cdot 100, \\ \epsilon_{amplitude}[\%] &= (1 - \cos(\Delta_J \cdot \pi \cdot f)) \cdot 100 \end{aligned} \tag{16}$$

Both errors are shows in Table 15.

In the frequency domain, the amplitude of vibration remains unaffected because of the incoherent averaging.

Table 15. *Error from the digital signal output jitter.*

f	ϵ_{phase}[%]	$\epsilon_{amplitude}$[%]
1 Hz	790f%	4µ%
10 Hz	79p%	40µ%
100 Hz	7.9n%	400µ%
1 kHz	790n%	4m%
10 kHz	79µ%	40m%
100 kHz	7.9m%	400m%
1 MHz	789m%	4%
2.5 MHz	4.9%	10%

INTERFACES

Front plate

Figure 5. *Front plate layout*

1. Environmental Module
An Environmental Module from SmarAct Metrology GmbH & Co. KG can be used to compensate for environmental changes and increase measurement accuracy.

2. Laser
FC-APC mate in which a sensorhead must be inserted.

3. Pilot Laser
Activates or deactivates the pilot laser.

4. Power Button
Power switch controlling the controller.

Back plate

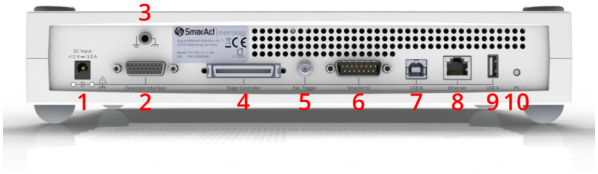

Figure 6. *Back plate layout*

1. DC power supply connector
The system controller is powered with a 12 V the provided original AC/DC power supply. System ground is connected to protective earth (PE) inside the external AC/DC power supply. The power consumption is below 30 W.

2. Extension Interface
Reserved for future use.

3. System ground
A 4 mm banana socket can be connected to system ground and to bring several devices to the same electrical potential.

4. Stage Controller
The system controller has a mini ribbon 50 connector which provides several interfaces including analog and digital GPIOs as well as Digital Differential Interfaces (DDI) to be accessible via the stage controller. A 100 ohm termination resistor is implemented before the mini ribbon 50 connector.

5. External trigger input
The SMA connector can be used to input a digital signal in order to trigger internal processes.

6. SmarAct Sensor Interface (SI)
Reserved for future use.

7. USB B
To configure the system controller Controller the system has to be connected to a PC. Therefore, a USB 2.0 cable can be connected here and the connection can be established with the graphical user interface, for example. The USB interface is one of the main bidirectional communication interfaces of the system controller. It provides a USB 2.0 high speed connection with data rates of up to 480 Mbits/s.

8. Ethernet
The Ethernet interface is the second main bidirectional communication interface of the system controller. The interface is configured via the embedded PC and is able to provide Gigabit Ethernet.

9. USB A
The USB 2.0 host interface is used for software updates and diagnostic snapshots via an USB stick.

10. PS
For firmware upgrade.

LASER SAFETY

The system controller is a Class 1 laser product. Because of its special properties, laser light poses safety hazards not associated with light from conventional sources. Even though the system controller is inherently eye-safe, it is good practice to avoid direct exposure to human eye and skin, and ensure the optical path is well controlled. Furthermore, optical ports shall always be covered with the protective caps, when unused. (This also protects them from contamination

and permanent damage.) The safe use of the laser depends upon the user being familiar with the instrument and the properties of laser radiation.

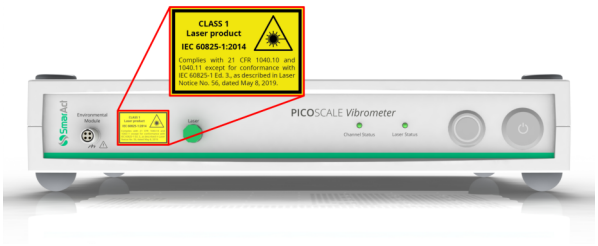

Figure 7. *Laser safety label on the front panel of the Controller.*

Output parameters

The system controller Controller contains an infrared diode laser (1530–1560nm) and an additional pilot laser (640–660nm) which output powers are given in Table 16. In case a -3dB attenuator is used, the powers are halved.

Table 16. *system controller Laser maximum output powers for the two wavelengths at the system controller laser output.*

Wavelength	(640–660nm)	(1530–1560nm)
Typical Power	350 µW	1.8 mW
Typical Power, -3dB	175 µW	0.9 mW

DIMENSIONS AND CONDITIONS

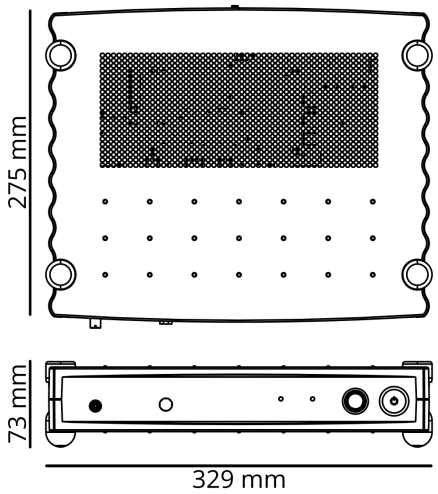

Figure 8. *Controller Dimensions. Weight 3.7 kg.*

Table 17. *Operation conditions for* **PICO**SCALE *Controller.*

Property	Parameter
Degree of Pollution (acc. to EN 60664-1:2007)	2
Power supply	12 V DC ±5 %
Input current	3.0 A
Operation temperature	15 °C - 30 °C ±2.5 °C dynamic*
Relative humidity	20% to 80% RH non-condensing
Storage temperature	0 °C - 50 °C
Transport temperature	0 °C - 50 °C
Altitude	up to 2000 m

*Maximum temperature fluctuations during measurement that guarantee performance.

Completeness of contents

The hazards and warnings listed in this section are incomplete. Before operation, the user has to read the user manual, which contains more safety information.

ORDER CODES

The order codes of the system controller and its accessories are given in Table 18.

Table 18. *Order codes of the system controller and accessories.*

Order code	Description
PV-CTRL-V1.5-TAB	**PICO**SCALE *Vibrometer* system controller including fiber optic attenuator
FA03T-APC	Fiber optic attenuator 3 dB

Contact

Germany

SmarAct Metrology GmbH & Co. KG

August-Wilhelm-Kuenholz-Str. 1
D-26135 Oldenburg
Germany

T: +49 441 - 800 879 0
Email: metrology@smaract.com
www.smaract.com

France

SmarAct GmbH

Schuette-Lanz-Strasse 9
26135 Oldenburg
Germany

T: +49 441 - 800 879 956
Email: info-fr@smaract.com
www.smaract.com

USA

SmarAct Inc.

2140 Shattuck Ave. Suite 302
Berkeley, CA 94704
United States of America

T: +1 415 - 766 9006
Email: info-us@smaract.com
www.smaract.com

China

Dynasense Photonics

6 Taiping Street
Xi Cheng District,
Beijing, China

T: +86 10 - 835 038 53
Email: info@dyna-sense.com
www.dyna-sense.com

Natsu Precision Tech

Room 515, Floor 5, Building 7,
No.18 East Qinghe Anning
Zhuang Road,
Haidian District
Beijing, China

T: +86 18 - 616 715 058
Email: chenye@nano-stage.com
www.nano-stage.com

Shanghai Kingway Optech Co.Ltd

Room 1212, T1 Building
Zhonggeng Global Creative Center
Lane 166, Yuhong Road
Minhang District
Shanghai, China

Tel: +86 21 - 548 469 66
Email: sales@kingway-optech.com
www.kingway-optech.com

Japan

Physix Technology Inc.

Ichikawa-Business-Plaza
4-2-5 Minami-yawata,
Ichikawa-shi
272-0023 Chiba
Japan

T/F: +81 47 - 370 86 00
Email: info-jp@smaract.com
www.physix-tech.com

South Korea

SEUM Tronics

1109, 1, Gasan digital 1-ro
Geumcheon-gu
Seoul, 08594,
Korea

T: +82 2 - 868 10 02
Email: info-kr@smaract.com
www.seumtronics.com

Israel

Optics & Motion Ltd.

P.O.Box 6172
46150 Herzeliya
Israel

T: +972 9 - 950 60 74
Email: info-il@smaract.com
www.opticsmotion.com

SmarAct Metrology GmbH & Co. KG develops sophisticated equipment to serve high accuracy positioning and metrology applications in research and industry within fields such as optics, semiconductors and life sciences. Our broad product portfolio – from miniaturized interferometers and optical encoders for displacement measurements to powerful electrical nanoprobers for the characterization of smallest semiconductor technology nodes – is completed by turnkey scanning microscopes which can be used in vacuum, cryogenic or other harsh environments.
We maintain the complete production in house for a high level of customization so that we can always provide you the optimal individual or OEM solution. We also offer feasibility studies, measurement services and comprehensive support to accompany you along your projects.

Headquarters

SmarAct GmbH
Schuette-Lanz-Strasse 9
26135 Oldenburg
Germany

T: +49 441 - 800 879 0
Email: info-de@smaract.com
www.smaract.com

USA

SmarAct Inc.
2140 Shattuck Ave. Suite 302
Berkeley, CA 94704
United States of America

T: +1 415 - 766 9006
Email: info-us@smaract.com
www.smaract.com